IEEE Access
Multidisciplinary | Rapid Review | Open Access Journal

Received September 12, 2021, accepted September 23, 2021, date of publication September 27, 2021,
date of current version October 5, 2021.

Digital Object Identifier 10.1109/ACCESS.2021.3115944

Optimal Control Method and Design for Modular Battery Energy Storage System Based on Partial Power Conversion

KAIYUAN ZHENG, WEIGE ZHANG, XUEZHI WU, (Member, IEEE), AND LONG JING
School of Electrical Engineering, Beijing Jiaotong University, Haidian, Beijing 100044, China
National Active Distribution Network Technology Research Center (NANTEC), Beijing Jiaotong University, Beijing 100044, China

Corresponding author: Xuezhi Wu (xzhwu@bjtu.edu.cn)

This work was supported by the Delta Power Electronics Science and Education Development Program of Delta Group under Grant BS123456.

ABSTRACT This article addresses a bidirectional low power loss series-parallel partial-power modular converter (SPPC) suitable for series-connected high voltage large power battery energy storage system (BESS). A specific capacitor is placed on the top of the series battery packs, which voltage can be adjusted by the SPPC to compensate for the voltage fluctuation of the battery packs and the DC power line. The power loss and cost of the SPPC are relatively low since its rated power is reduced to about $22\% - 48\%$ of the full-power converter. A 3 level distributed control method is proposed to achieve the fast transient response of the DC power line current and deal with the series inconsistency of battery packs during discharging and charging, further improving the total energy utilization efficiency (EUE) of the BESS. The critical design considerations for SPPC-BESS are analyzed. A bidirectional 800W phase-shift full-bridge (PSFB) converter hardware prototype along with the Gallium Nitride (GaN) devices is provided to verify the high efficiency of DC-DC sub-module. Then a simulation model of a 6.6kW SPPC-BESS with 3 sub-modules to verify the feasibility of the control method. Theoretical analysis proves that the total power loss of the SPPC is lower than the existing types of modular converters. The EUE of the SPPC-BESS is 1.7% higher than the conventional BESS when the average maximum available capacities of batteries attenuate to 80% of the initial maximum available capacity.

INDEX TERMS Energy utilization efficiency, partial power modular converter, battery energy storage system, smart battery unit, distributed control strategy.

I. INTRODUCTION

Lithium-ion (Li-ion) batteries have become popular due to their high energy and power density, no memory effect, pollution-free operation, and low self-discharge rate [1]. Li-ion BESS can provide power for the DC power line independently and rapidly and be widely used in the micro-grid [2], electric vehicles (EVs) [3], [4], data centers DC distribution energy storage [5], rail system [6], and automated guided vehicle fully-automated system in port terminals [7], [8], etc. The efficient utilization of energy hinges on cost-effect and efficient BESS.

Due to the limitations of the anode and cathode materials, Li-ion cells can only produce a limited voltage operation range, e.g., from 2.2V to 3.65V for $LiFePO_4$ batteries; from 1.5V to 2.7V for $Li_4Ti_5O_{12}$ batteries [9], which cannot meet the requirements for the voltage and power [10]. A battery pack consists of hundreds and thousands of Li-ion cells, connected in series to form the series battery branch, satisfying the voltage requirement. The series battery branch is then paralleled to extend the scope of current.

A bidirectional DC-DC converter is added to a BESS to control discharging or charging power, as shown in Fig. 1. The two-level buck/boost topology is for the 750V medium voltage BESS [11] and the three-level topology is for the 1500V high voltage BESS [12]. Although simple structure, high power conversion efficiency, low cost, mature control of the conventional BESS, the EUE of the series battery packs is dramatically reduced after hundreds of operation cycles due to the low consistency of battery parameters such as available capacity, the state of charge (SOC), and resistance [13].

The associate editor coordinating the review of this manuscript and approving it for publication was Zhilei Yao.

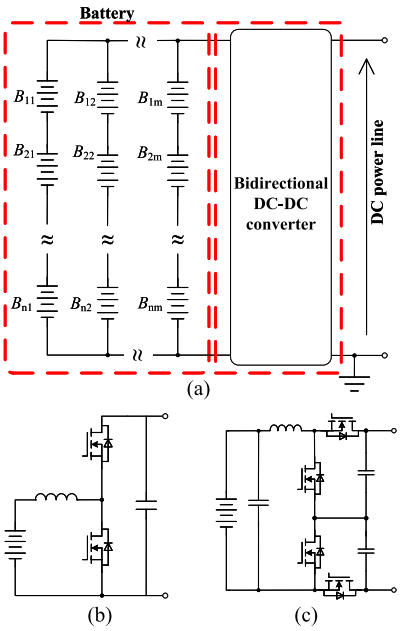

FIGURE 1. The conventional full-power BESS diagram. (a) BESS diagram. (b) Two-level converter. (c) Three-level converter.

In these situations, the battery packs parallel-connection is more efficient than the series-connection to increase the EUE of battery packs. References [14] summarizes non-isolated high-step-up converter topology based on the parallel-connected configuration. However, the maximum voltage gain of those converters is limited to about 1:5 by the high current ripple and the extreme duty cycle, which is not suitable for high voltage applications.

In order to achieve high EUE under wider voltage range, modular BESS is proposed, solving the ''short board effect'' of series batteries. The conventional series-connection architecture of battery packs is replaced by grouping, reducing the number of series-connected Li-ion cells in one group. References [15] verifies that the EUE of modular BESS can be improved by 10.21% through a specific active equalization strategy. The converter efficiency decreases as the increase of group number on the same power. Further, [16] proves that there is the optimal group number, which makes the EUE maximize on the given capacity distribution among batteries.

Although existing modular BESS can achieve a higher EUE of batteries, full-power operation increases the loss and cost of the power converter. The concept of partial power conversion was first proposed in photovoltaic (PV) systems [17], [18], that enable each PV element to operate at its maximum power point while processing only a small fraction of the total power produced. References [19] proposed a partial power topology for the PV system that combines the series and parallel connection, increasing scalability. References [20] applies the series-parallel partial power topology (SPPC) to a set-up power converter with two Li-ion cells in portable device, integrating the balancing feature and has a smaller overall volume of the reactive components. However its results cannot prove that the SPPC topology is feasible for a high voltage and high power BESS, which imposes challenges.

1) A large number of series batteries make the inconsistency more serious than in portable devices with the increase of service time. The series batteries are divided into several groups. The control method becomes complex to process output power and energy second dispatch of battery packs according to capacities, SOCs, and resistances.

2) The design of the SPPC-BESS should compromise the energy utilization of battery packs and the power loss of the SPPC. Therefore, the optimal grouping number, transformer ratio, and the DC-DC sub-module's input/output voltage range need to be selected carefully.

3) BESS operates in constant voltage (CV) mode most of the time. The charging current is small, requiring high-efficiency DC-DC at light load.

Saving a fraction of that power is more significant for high voltage and high power BESS. Therefore the SPPC-BESS is a better choice for the high voltage and high power BESS than the full power topology since its low power loss. Simplifying and optimizing control method and design is a worthwhile study that will help deploy the SPPC to different applications.

This article is organized as follows. Section II introduces the structure and principles of the proposed SPPC-BESS. Section III provides a 3 level control method to achieve the fast transient response for the DC power line and equalization of battery packs. Section IV analysis the design considerations of the SPPC-BESS. Section V validates the high efficiency of the DC-DC sub-module by an 800W bidirectional PSFB prototype. Section VI provides a simulation model for the 6.6kW SPPC-BESS to verify the dynamic performance and equalization results. Section VII give the analysis of the EUE for 4 types of BESSs.

II. STRUCTURE OF THE SPPC-BESS

A. THE CONCEPT OF THE SMART BATTERY

The smart battery (SB) concept is put forward in this article based on modular BESS architecture and the distributed control of battery packs. A modular BESS consists of n SB units. The SB units possess the same structure, consisting of a battery pack and its paralleled DC-DC sub-module, shown in Fig. 2. The output power of one battery pack can be controlled independently by its DC-DC sub-module. So that one SB unit can be viewed as a local current source. The equalization strategy for the BESS can be achieved by output currents ($i_{SB,1}$, $i_{SB,2}$, . . . , $i_{SB,n}$) allocation during discharging and charging.

The modular BESS based on the SB concept has merits, including flexibility and reliability. A BESS can be quickly formed to meet different power and voltage requirements in various applications by changing the SBs connection. The connection modes of SBs include the input series and output parallel (ISOP), the input parallel and output series (IPOS), input series and output series (ISOS), the input parallel and output parallel (IPOP) and the series-parallel connection.

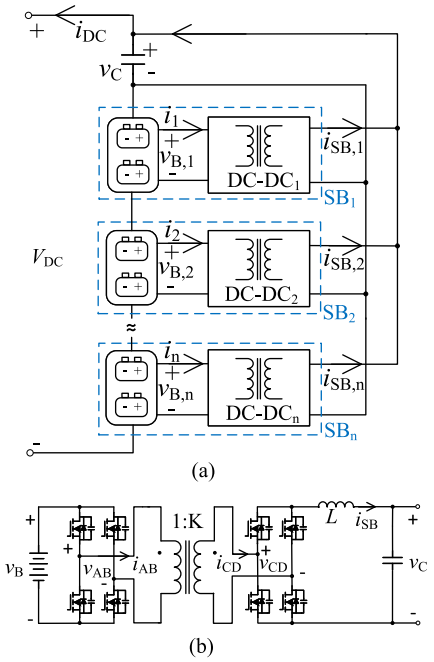

FIGURE 2. Topology of the SPPC-BESS and the DC-DC sub-module. (a) The SPPC-BESS topology. (b) The PSFB bidirectional DC-DC topology.

These diverse connection modes are beneficial to the scalability of the BESS. What's more, fault diagnosis and redundancy based on the SB unit improve system reliability, does not discussed in this article.

B. THE TOPOLOGY OF THE SPPC-BESS

The SPPC-BESS consists of SB units connected in series-parallel mode, shown in Fig. 2 (a). By controlling the voltage of output capacitor v_C, the real-time compensation for the series battery packs' voltage changes can be achieved. The equalization strategies are executed during discharging and charging.

Equation (1), (2) represent the calculation of v_C and i_{DC}.

$$v_C(t) = v_{DC}(t) - \sum_{i=1}^{n} v_{B,i}(t) \tag{1}$$

$$i_{DC}(t) = \sum_{i=1}^{n} i_{SB,i}(t) \tag{2}$$

v_C is the output capacitor voltage of the SPPC; v_{DC} is the DC power line voltage, fluctuated in a small range. i_{DC} is the current of the DC power line. $i_{SB,i}$ is the output current of SB$_i$, $i_{B,i}$ is the discharging current of the battery pack i, where i = 1, 2, . . . , n.

Equation (3) illustrates the current function of battery pack i.

$$i_{B,i}(t) = i_i(t) + i_{DC}(t) \tag{3}$$

$i_{B,i}$ is the discharge current of battery pack i; i_i is the input current of the DC-DC$_i$, i = 1, 2, . . . , n.

The operation power of the SPPC is associated with v_C and i_{DC}, shown in (4), (5).

$$p_C = v_C \cdot i_{DC} \tag{4}$$

$$P_{CN} = V_{CN} \cdot I_N \tag{5}$$

I_N is the rated output current of the SPPC-BESS, P_{CN} is the rated power of the SPPC.

Whereas the rated power of the SPPC-BESS P_N can be defined as (6).

$$P_N = V_{DC}^{max} \cdot I_N \tag{6}$$

V_{DC}^{max} is the maximum value of the DC power line voltage. This article defines δ as the power proportion of the SPPC.

$$\delta = \frac{P_{CN}}{P_N} = \frac{V_{CN}}{V_{DC}^{max}} \tag{7}$$

The lower-rated power of the SPPC can be achieved about δ of the full-power converter. It can be considered that $\delta \ll 1$. The calculation of δ will be discussed in section IV in detail. Therefore the cost of the converter was reduced greatly.

The total power loss of the SPPC can be denoted as (8).

$$p_{loss} = P_{CN} \cdot (1 - \eta_C) \tag{8}$$

η_C is the DC-DC sub-module efficiency.

Even if the efficiency of the DC-DC sub-module lower than the full power converter, the total power loss of the SPPC is reduced since $P_{CN} \ll P_N$.

C. THE TOPOLOGY OF THE DC-DC SUB-MODULE

The isolated DC-DC topology is essential for the SPPC since series-parallel architecture, divided into three types: the PSFB converter, the dual active bridge (DAB) converter [21], [22], and the LLC-type converter [23]. In most of the operation time of a BESS, the battery works in constant voltage (CV) mode with a small charging current. The high efficiency at light load and the stability are the crucial factors. DAB circuit has low efficiency at light load since the circulating current. The LLC converter has the highest efficiency due to all switches are soft switching by resonant. However, the control is too complex to applied in BESS. The PSFB achieves current control by phase-shift strategy with strong robustness, and the efficiency at light load is especially high. Therefore, the PSFB bidirectional DC-DC is adopted as the sub-module for the SPPC, as shown in Fig. 2 (b).

The relationship of input and output ports of the DC-DC$_i$ is shown as (9).

$$\begin{bmatrix} v_{B,i} \\ i_i \end{bmatrix} = \begin{bmatrix} \frac{1}{K \cdot d_i} & 0 \\ 0 & K \cdot d_i \end{bmatrix} \cdot \begin{bmatrix} v_C \\ i_{SB,i} \end{bmatrix} \tag{9}$$

v_C and $i_{SB,i}$ are regulated by the duty cycle d_i like a traditional DC-DC.

This article defines $K_{SB,i}$ as the voltage gain of the DC-DC sub-module as shown in (10).

$$K_{SB,i} = \frac{v_C}{v_{B,i}} \tag{10}$$

The relationship between the battery current and the output current of the DC-DC sub-module can be calculated as (11).

$$i_{\mathrm{B,i}}(t) = K_{\mathrm{SB,i}} \cdot i_{\mathrm{SB,i}}(t) + i_{\mathrm{DC}}(t) \tag{11}$$

If different DC-DC topologies are adopted such as DAB and LLC, the modulation strategy is different from the BUCK/BOOST topology. However, the system control strategy will not be changed if only the input and output current and voltage relationships are confirmed.

III. CONTROL METHOD OF THE SPPC-BESS

Partial power conversion schemes for BESS are proposed successively [29]–[32]. However, both the grouping and the inconsistency of series battery packs are not taken into consideration. There are few articles that make an intensive study about the control method for partial power conversion of modular series BESS. Although distributed control strategies with equalization for modular BESS have been proposed in [33]–[35], these control strategies does not involve partial power conversion.

There are several challenges to the control method facing the adoption of the SPPC-BESS structure.

1) The sub-modules' output terminals are connected together in parallel and then series with its input in the SPPC. Therefore the power control of the SPPC-BESS is a challenge since the decoupling between the output and the input should be achieved.

2) Multiple optimization objectives for a series battery pack, including consistent SOCs, available residential capacities, and available residential energy maximize, make the optimal control of the BESS different from MPPT in a photovoltaic system. The partial power control strategy should integrate the equalization between battery packs into the power control of the DC power line by different battery optimization objectives.

3) Distributed control strategies are adopted for the SPPC-BESS to achieve the flexible configuration of battery packs, fault detection, and redundancy functions. The partial power conversion and the equalization control are performed in each sub-module independently without global coordinating.

In order to solve the above problems, this article proposes a distributed control method with an active equalization for the SPPC-BESS. The control strategy is divided into 3 levels by different time scales to achieve power control and equalization. Optimization objectives of battery packs can be embedded into the control strategy to realize an active equalization strategy. Distributed control strategy is adopted to improve system scalability.

The maximum available capacity of one battery is defined as the available capacity on the minimal discharging (or charging) current. Take $Q_{\mathrm{i}}^{\mathrm{D}}$ as the residual discharging capacity of battery pack i and $Q_{\mathrm{i}}^{\mathrm{C}}$ as the residual charging capacity of battery pack i, which are defined by (12), (13).

$$Q_{\mathrm{i}}^{\mathrm{D}}(t) = SOC_{\mathrm{i}}(t) \cdot Q_{\mathrm{i}}^{\max} \tag{12}$$

$$Q_{\mathrm{i}}^{\mathrm{C}}(t) = (1 - SOC_{\mathrm{i}}(t)) \cdot Q_{\mathrm{i}}^{\max} \tag{13}$$

$SOC_{\mathrm{i}}(t)$ is the state of charge of battery pack i. $Q_{\mathrm{i}}^{\max}(t)$ is the maximum available capacity of battery pack i. The relationship of $Q_{\mathrm{i}}^{\mathrm{D}}(t)$ and $Q_{\mathrm{i}}^{\mathrm{C}}(t)$ is shown in (14). They are a pair of complementary variables. During discharging and charging, they are regarded as control targets respectively.

$$Q_{\mathrm{i}}^{\mathrm{C}}(t) + Q_{\mathrm{i}}^{\mathrm{D}}(t) = Q_{\mathrm{i}}^{\max} \tag{14}$$

The residual discharging (and charging) capacity can be obtain by ampere hour integral according to (15), (16).

$$Q_{\mathrm{i}}^{\mathrm{D}}(t) = Q_{\mathrm{i}}^{\mathrm{D}}(t0) - \int_{t0}^{t} i_{\mathrm{B,i}}(t)dt \tag{15}$$

$$Q_{\mathrm{i}}^{\mathrm{C}}(t) = Q_{\mathrm{i}}^{\mathrm{C}}(t0) + \int_{t0}^{t} i_{\mathrm{B,i}}(t)dt \tag{16}$$

Then the distributed variables are defined for active equalization in this article, shown in (17), (18), (19), (20).

$$Q_{\mathrm{i}}^{\mathrm{equ}}(t) = \begin{cases} \overline{Q^{\mathrm{D}}(t)} - Q_{\mathrm{i}}^{\mathrm{D}}(t), & i_{\mathrm{DC}}(t) > 0 \\ \overline{Q^{\mathrm{C}}(t)} - Q_{\mathrm{i}}^{\mathrm{C}}(t), & i_{\mathrm{DC}}(t) < 0 \end{cases} \tag{17}$$

$$i_{\mathrm{B,i}}^{\mathrm{equ}}(t) = \overline{i_{\mathrm{B}}(t)} - i_{\mathrm{B,i}}(t) \tag{18}$$

$$i_{\mathrm{SB,i}}^{\mathrm{equ}}(t) = \overline{i_{\mathrm{SB}}(t)} - i_{\mathrm{SB,i}}(t) \tag{19}$$

$$i_{\mathrm{i}}^{\mathrm{equ}}(t) = \overline{i(t)} - i_{\mathrm{i}}(t) \tag{20}$$

where,

$$\overline{Q^{\mathrm{D}}(t)} = \frac{1}{\mathrm{n}} \cdot \sum_{\mathrm{i}=1}^{\mathrm{n}} Q_{\mathrm{i}}^{\mathrm{D}}(t) \tag{21}$$

$$\overline{Q^{\mathrm{C}}(t)} = \frac{1}{\mathrm{n}} \cdot \sum_{\mathrm{i}=1}^{\mathrm{n}} Q_{\mathrm{i}}^{\mathrm{C}}(t) \tag{22}$$

$$\overline{i_{\mathrm{B}}(t)} = \frac{1}{\mathrm{n}} \cdot \sum_{\mathrm{i}=1}^{\mathrm{n}} i_{\mathrm{B},i}(t) \tag{23}$$

$$\overline{i_{\mathrm{SB}}(t)} = \frac{1}{\mathrm{n}} \cdot \sum_{\mathrm{i}=1}^{\mathrm{n}} i_{\mathrm{SB,i}}(t) \tag{24}$$

$$\overline{i(t)} = \frac{1}{\mathrm{n}} \cdot \sum_{\mathrm{i}=1}^{\mathrm{n}} i_{\mathrm{i}}(t) \tag{25}$$

$Q_{\mathrm{i}}^{\mathrm{equ}}(t)$ represents the equalization capacity of battery pack i. It reflects the difference between the average residual discharging (or charging) capacity of all battery packs and the individual residual discharging (or charging) capacity of one battery pack.

The equalization strategy of the SPPC-BESS in this article can be described as follow:

The SPPC-BESS starts the discharging (or charging) at time $t0$ and ends the discharging (or charging) at t_{end}. Assume that at time t_{end}, the SPPC-BESS is fully discharged (or charged). Then, define $\Delta T = t_{\mathrm{end}} - t0$ as the total operation time. The basic principle of SOC equalization between battery packs can be described as follow:

At time t_{end}, $\forall i \in [1, \mathrm{n}]$, $Q_{\mathrm{i}}^{\mathrm{equ}}(t_{\mathrm{end}}) = 0$.

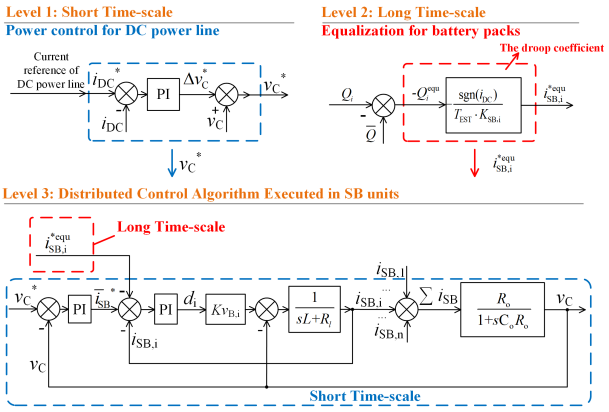

FIGURE 3. The distributed control strategy diagram for the SPPC-BESS.

That means that all the battery packs in the SPPC-BESS are fully discharged (or charged) when the discharging (or charging) ends. The capacity of all the battery packs can be fully used.

According to (11) and the definition of equalization variables, there is,

$$i_{\mathrm{B,i}}^{\mathrm{equ}}(t) = K_{\mathrm{SB,i}} \cdot i_{\mathrm{SB,i}}^{\mathrm{equ}}(t) \tag{26}$$

Equation (26) proves that $i_{\mathrm{SB,i}}^{\mathrm{equ}}(t)$ changes linearly with $i_{\mathrm{B,i}}^{\mathrm{equ}}(t)$. A distributed control strategy is proposed for the SPPC-BESS based on the 3 level architecture, shown in Fig. 3.

where C_{o} is the output capacitance. R_l is the equivalent resistance of the output inductance. R_{o} is the equivalent resistance of the DC power line. T_{EST} is an estimated value of ΔT.

In the SPPC-BESS, the DC power line current i_{DC} is the control target. The DC power line voltage can also be the control target in off-line supply mode, which is not discussed in this article. (27) shows that i_{DC} is decided by the little difference between the output voltage of the BESS and the DC power line since the resistance of the DC power line is very small.

$$i_{\mathrm{DC}}(t) = \frac{v_{\mathrm{C}}(t) + \sum_{\mathrm{i=1}}^{\mathrm{n}} v_{\mathrm{B,i}}(t) - v_{\mathrm{DC}}(t)}{R_{\mathrm{o}}} \tag{27}$$

On level 1, $i_{\mathrm{DC}}(t)$ is regulated by the feedback controller. The proportional-integral (PI) regulator is to guarantee the rapid response of i_{DC}. Then the output of the PI regulator is transformed to the increment of v_{C}^{*}.

Energy second dispatch between the battery packs is achieved on level 2. The SOC and discharging (or charging) current of battery packs have similar droop characteristics to the smart grid for distributed energy resources [25]. The distributed droop control strategy is adopted to achieve the currents assignment between battery packs.

At the time $t0$, the equalization algorithm is executed the first time. Then there is,

$$Q_{\mathrm{i}}^{\mathrm{D}}(t_{\mathrm{end}}) = Q_{\mathrm{i}}^{\mathrm{D}}(t0) - \int_{t0}^{t0+T_{\mathrm{EST}}} i_{\mathrm{B,i}}(t)dt \tag{28}$$

$$\overline{Q^{\mathrm{D}}(t_{\mathrm{end}})} = \overline{Q^{\mathrm{D}}(t0)} - \int_{t0}^{t0+T_{\mathrm{EST}}} \overline{i_{\mathrm{B,i}}}(t)dt \tag{29}$$

$$Q_{\mathrm{i}}^{\mathrm{C}}(t_{\mathrm{end}}) = Q_{\mathrm{i}}^{\mathrm{C}}(t0) + \int_{t0}^{t0+T_{\mathrm{EST}}} i_{\mathrm{B,i}}(t)dt \tag{30}$$

$$\overline{Q^{\mathrm{C}}(t_{\mathrm{end}})} = \overline{Q^{\mathrm{C}}(t0)} + \int_{t0}^{t0+T_{\mathrm{EST}}} \overline{i_{\mathrm{B,i}}}(t)dt \tag{31}$$

where,

$$T_{\mathrm{EST}} = t_{\mathrm{end}} - t0 \tag{32}$$

Let $Q_{\mathrm{i}}^{\mathrm{equ}}(t_{\mathrm{end}}) = 0$, there is,

$$Q_{\mathrm{i}}^{\mathrm{equ}}(t0) = \mathrm{sgn}(i_{\mathrm{DC}}(t0)) \cdot \int_{t0}^{t0+T_{\mathrm{EST}}} i_{\mathrm{B,i}}^{\mathrm{equ}}(t)dt \tag{33}$$

Assuming that $i_{\mathrm{B,i}}(t) = i_{\mathrm{B,i}}(t0)$ when $t \in (t0, t_{\mathrm{end}})$, there is,

$$i_{\mathrm{B,i}}^{\mathrm{equ}}(t0) = \mathrm{sgn}(i_{\mathrm{DC}}(t0)) \cdot \frac{1}{T_{\mathrm{EST}}} \cdot Q_{\mathrm{i}}^{\mathrm{equ}}(t0) \tag{34}$$

Bring (26) into (34), the equalization output current reference of the DC − $\mathrm{DC_i}$ can be expressed as (35).

$$i_{\mathrm{SB,i}}^{\mathrm{equ}}(t0) = \mathrm{sgn}(i_{\mathrm{DC}}(t0)) \cdot \frac{1}{K_{\mathrm{SB}} \cdot T_{\mathrm{EST}}} \cdot Q_{\mathrm{i}}^{\mathrm{equ}}(t0) \tag{35}$$

$Q_{\mathrm{i}}^{\mathrm{equ}}(t0)$ is viewed as the reference value of $Q_{\mathrm{i}}^{\mathrm{equ}}$ in the next equalization period, assigned to the $i_{\mathrm{B,i}}^{\mathrm{equ}*}$ by a droop coefficient $1/(K_{\mathrm{SB,i}} \cdot T_{\mathrm{EST}})$.

T_{EST} can be calculated according to (36).

$$T_{\mathrm{EST}} = \Delta t \cdot \frac{Q_{\mathrm{i}}(t)}{Q_{\mathrm{i}}(t - \Delta t) - Q_{\mathrm{i}}(t)} \tag{36}$$

Δt is the execution time interval of the twice equalization strategy.

IV. DESIGN CONSIDERATION OF THE SPPC-BESS

A. BOUNDARY CONDITIONS

The series battery pack voltage satisfies the boundary condition, shown in (37).

$$\mathrm{n} \cdot V_{\mathrm{B}}^{\min} < \sum_{i=1}^{n} v_{\mathrm{B,i}} < \mathrm{n} \cdot V_{\mathrm{B}}^{\max} \tag{37}$$

$V_{\mathrm{B}}^{\min}$ and $V_{\mathrm{B}}^{\max}$ are the lower and upper limit voltage of the battery packs. $v_{\mathrm{B,i}}$ is the terminal voltage of the battery pack i. n is the number of series battery packs.

In the initiated stage of operating, the Li-ion cells in one battery pack are consistent. The battery pack's terminal voltage can be viewed as the sum voltage of the Li-ion cells. Similarly, the battery pack's upper and lower limit voltage can be calculated by the Li-ion cells' limit voltage approximately. Defining β as the usable scope proportion of series battery packs' voltage, shown in (38).

$$\beta = \frac{V_{\mathrm{CELL}}^{\max} - V_{\mathrm{CELL}}^{\min}}{V_{\mathrm{CELL}}^{\max}} = \frac{\Delta V_{\mathrm{B}}}{V_{\mathrm{B}}^{\max}} \tag{38}$$

where,

$$\Delta V_{\mathrm{B}} = V_{\mathrm{B}}^{\max} - V_{\mathrm{B}}^{\min} \tag{39}$$

ΔV_{B} is the voltage scope of battery pack.

$V_{\mathrm{CELL}}^{\max}$ is the upper limit voltage, $V_{\mathrm{CELL}}^{\min}$ is the lower limit voltage of the Li-ion cell, which the battery manufacturer provides. This paper takes $Li_4Ti_5O_{12}$ batteries as the basis of analysis. The operation voltage range of the Li-ion cell is between 2V and 2.7V. That is, $V_{\mathrm{CELL}}^{\max}$ is equal to 2.7V and $V_{\mathrm{CELL}}^{\min}$ is equal to 2V. Then, $\beta = 0.26$.

The DC power line fluctuates in a certain range during operation. The boundary condition of the DC power line is shown in (40).

$$V_{\mathrm{DC}}^{\min} < v_{\mathrm{DC}} < V_{\mathrm{DC}}^{\max} \tag{40}$$

$V_{\mathrm{DC}}^{\max}$ is the maximum voltage, and $V_{\mathrm{DC}}^{\min}$ is the minimum voltage of the DC power line. Defining α as the fluctuation scope proportion of DC power line voltage, shown in (41).

$$\alpha = \frac{\Delta V_{\mathrm{DC}}}{V_{\mathrm{DC}}^{\max}} \tag{41}$$

where,

$$\Delta V_{\mathrm{DC}} = V_{\mathrm{DC}}^{\max} - V_{\mathrm{DC}}^{\min} \tag{42}$$

ΔV_{DC} is the voltage scope of the DC power line.

B. CONSTRAINT EQUATIONS

The minimum value of v_{C} can be defined as V_{C0}; The maximum value of v_{C} can be defined as V_{CN}. From the DC power line, v_{C} reached its minimum value V_{C0} when the DC power line voltage fluctuated to its lowest value, and all of the battery packs' voltage reaches its upper limit voltage value nearing fully charged state; Whereas v_{C} reached its maximum value V_{CN} when the DC power line voltage fluctuated to its highest value and the battery packs' voltage reaches its lower limit voltage value nearing fully discharged state; According to (1), the constraint function of the SPPC-BESS can be deduced as (43), (44).

$$V_{\mathrm{C0}} = V_{\mathrm{DC}}^{\min} - \mathrm{n} \cdot V_{\mathrm{B}}^{\max} \tag{43}$$

$$V_{\mathrm{CN}} = V_{\mathrm{DC}}^{\max} - \mathrm{n} \cdot V_{\mathrm{B}}^{\min} \tag{44}$$

For one SB unit, v_{C} and $v_{\mathrm{B,i}}$ are the output and input voltage. Its DC-DC sub-module adjusts these voltages in full range at rated current by designing proper K and changing duty cycle during operation. The constraint equation of the DC-DC sub-module can be deduced as (45), (46).

$$V_{\mathrm{C0}} = K \cdot V_{\mathrm{B}}^{\max} \cdot D^{\min} \tag{45}$$

$$V_{\mathrm{CN}} = K \cdot V_{\mathrm{B}}^{\min} \cdot D^{\max} \tag{46}$$

$D^{\min}$ and $D^{\max}$ are the minimum and maximum steady value of the duty cycle. According to the constraint equations, the design specifications can be deduced as (47), (48).

$$\frac{\mathrm{n}}{K} = D^{\max} \cdot \left(\frac{1}{\delta} - 1\right) \tag{47}$$

$$D^{\min} = D^{\max} \cdot \left[\frac{(1-\alpha)(1-\beta) - (1-\delta)}{\delta}\right] \tag{48}$$

It can be illustrated from (47) and (48) that the number of battery packs in the SPPC-BESS n, transformer ratio K, and the steady-state scope of duty cycle of the DC-DC sub-module decided by multiple factors, including the SPPC power proportion δ, the voltage fluctuation proportion of DC power line α, the maximum usable proportion of battery packs' voltage β and the maximum duty cycle $D^{\max}$ of the DC-DC sub-module. As long as α, β, and $D^{\max}$ are determined, the changing trend of n/K and $D^{\min}$ are the same according to δ for different BESSs, shown in Fig. 4.

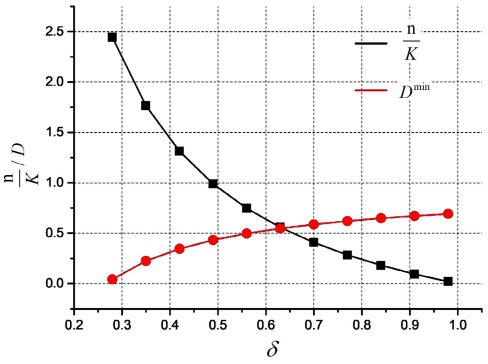

FIGURE 4. Design parameter for the SPPC-BESS.

TABLE 1. Design parameters of the SPPC-BESS.

Parameters	Value
Rated power of the SPPC-BESS P_{N}	6.6kW
Rated voltage of the DC power line	105V
Rated current of the SPPC-BESS I_{N}	60A
Range of i_{DC}	-60A∼60A
Battery type	$Li_4Ti_5O_{12}$
The maximum available capacity of battery	60Ah
Internal resistance	0.3mΩ
Battery upper limit voltage	2.7V
Battery open circuit voltage at 50% SOC	2.35V
Battery lower limit voltage	2.0V
α	0.01
β	0.26

where δ is the crucial index of the SPPC, representing the power proportion of the SPPC to BESS. For the same power BESS, a smaller δ is beneficial for decreasing the design power of the SPPC. The reduction of the design power shrinks both the cost and power loss of the converter. However, the smaller δ, the broader the duty cycle. Then the lower duty cycle for the DC-DC sub-module operation is inevitable, increasing dramatically conduct loss and the current stress of the low voltage side. That is, the smaller δ makes both the efficiency and stability of the DC-DC sub-module decrease.

Therefore, the SPPC-BESS design should compromise the reduction of the SPPC power and the optimal efficiency of the DC-DC sub-module.

C. THE DEFINATION OF EUE OF THE BESS

To verify the effect grouping on energy utilization of BESS, the concept of EUE [16] is used. The EUE in this article can be define as (49).

$$EUE = \frac{\sum_{\mathrm{i}=1}^{\mathrm{n}} e_{\mathrm{pack,\,i}}^{\mathrm{available}} - e_{\mathrm{loss,C}}}{\sum_{\mathrm{i}=1}^{\mathrm{n}} \sum_{\mathrm{j}=1}^{\mathrm{N}} E_{\mathrm{cell,\,j}}^{\max}} \tag{49}$$

where $e^{\text{available}}_{\text{pack, i}}$ is the available energy under a certain working condition; $E^{\max}_{\text{cell, j}}$ is the maximum available energy of Li-ion cell j in the battery pack; $e_{\text{loss,C}}$ is the energy loss of the power converter under a certain working condition; n is the number of the battery packs in the BESS and N is the number of series-connected Li-on cells in one battery pack. Assuming that the battery packs in the BESS reach the charging cut-off condition at $t = t0$ and begin to discharge. Finally this BESS reach its discharging cut-off condition at $t = t1$. The available energy during this discharging process can be denoted as (50).

$$e^{\text{available}}_{\text{pack, i}} = \int_{t0}^{t1} [i_{\text{B,i}}(t) \cdot U_{\text{OC,i}}(t) - i^2_{\text{B},i}(t) \cdot R_{\text{B},i}]dt \quad (50)$$

where $U_{\text{OC,i}}(t)$ is the open circuit voltage of the battery pack i. $i_{\text{B,i}}$ is the discharging current of the battery pack i. $R_{\text{B,i}}$ is the equivalent resistor of the battery pack i.

$$e_{\text{loss, C}} = \int_{t0}^{t1} p_{\text{loss}}dt \quad (51)$$

The optimization objective of the SPPC-BESS is the maximum of the EUE.

D. OPTIMAL DESIGN OF THE SPPC-BESS

A specific design case of the SPPC-BESS in this article is studied. Parameters are listed in Table 1. A simple test is introduced to analyze the optimal design. The SPPC-BESS discharging on 60A from the fully charged state at $t0$ and stop discharging at $t1$.

The efficiency of the PSFB DC-DC sub-module and power loss of the SPPC are firstly discussed. The rated output current, input and output voltages scope of the sub-module are varied with the δ and n. Then a series of the PSFB simulation models are established on the PLECS platform to analysis the efficiencies of different designs. The total power loss analysis of the SPPC is achieved when discharging the BESS. The PSFB DC-DC sub-module operates on the BUCK mode during discharging, and the power is delivered from one battery pack to the DC power line. The input voltage is varied from $V^{\max}_{\text{B}}$ to $V^{\min}_{\text{B}}$, the output voltage varied from V_{C0} to V_{CN}. The average value of operation efficiency at ($V^{\max}_{\text{B}}$, V_{C0}) and ($V^{\min}_{\text{B}}$, V_{CN}) is viewed as the discharging operation efficiency of the DC-DC sub-module in a specific design. The influence of equalization currents are ignored since they have a little contribution to the total power loss of the SPPC. The efficiency of the DC-DC sub-module and the total power loss of the SPPC are calculated, shown in Fig. 5 (a), (b).

For the same δ, there is a maximum efficiency value of the DC-DC converter with the increase of the grouping number. In this case, the efficiency is highest when the grouping number is 2.

For the same grouping number, the efficiency of the DC-DC sub-module increases with δ raises since the minimum duty cycle increases. In contrast, the total power loss of the SPPC decreases since the increasing of power of the SPPC.

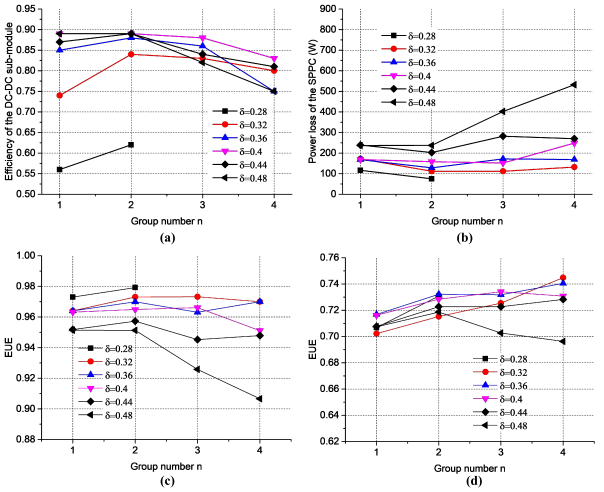

FIGURE 5. The relationship of the group number and the energy utilization of the SPPC-BESS. (a) The relationship of the group number and the average operation efficiency of the DC-DC sub-module at BUCK mode. (b) The relationship of the group number and the average discharging power loss of the SPPC. (c) The relationship of the group number and the EUE of the SPPC-BESS when there is no capacity attenuation of batteries. (d) The relationship of the group number and the EUE of the SPPC-BESS when the average capacity of batteries attenuates to 80% of the initial value.

The EUEs of the SPPC-BESS at all the design points are calculated, shown in Fig. 5 (c), (d). For the same δ, the EUE decreases as the grouping number increase due to the rise of power loss of the SPPC when the batteries' capacity consistent at the initial. Whereas the EUE increases as the grouping number increase due to the active equalization of battery packs when the average capacity of batteries attenuates to 80% and the standard deviation is 2.5% of the initial battery capacity.

The highest EUE is 74.5% achieved by the configuration $\delta = 0.32$ and $n = 4$ when the average capacity of batteries attenuates to 80% the initial battery capacity, which is improved by 4.26% compared to $n = 1$. Whereas the highest EUE is 97.9% achieved by the configuration $\delta = 0.28$ and $n = 2$ when the batteries' capacity consistent at the initial.

Therefore, the rise of the grouping number will be beneficial to the improvement of the EUE with poor battery consistency. However, increasing the grouping number brings additional converter losses. This article compromises equalization of the batteries and reducing power loss of the SPPC in the BESS design, choosing the optimal configuration $\delta = 0.32$ and $n = 3$.

V. THE 800W BIDIRECTIONAL DC-DC SUB-MODULE PROTOTYPE

GaN and Silicon Carbide (SiC) are the most mature among wide bandgap (WBG) semiconductors for high-power electronics. Although GaN offers better high-frequency performance, the lack of good-quality bulk substrates needed for vertical devices and lower thermal conductivity lend SiC a better position for high-voltage devices. In contrast, GaN technology has been maturing fast, applied for

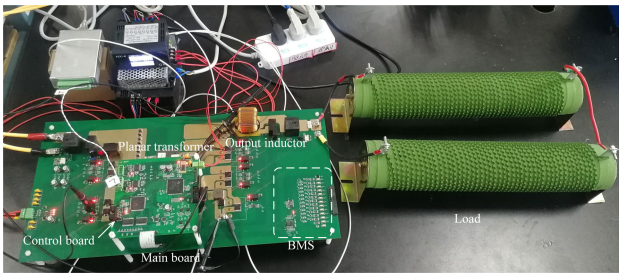

FIGURE 6. GaN-based 800 PSFB bidirectional DC-DC prototype.

TABLE 2. Parameters of the DC-DC sub-module.

Parameter	Value/type
P_{SBN} (rated power)	800W
V_{B} (input voltage)	36V
V_{CN} (rated output voltage)	40V
I_{SBN} (rated current)	20A
L (output inductance)	60uH
K (ratio of the transformer)	1.5
Micro-controller type	TMS320F28335
GaN device type	GS61008T
f_{s} (switch frequency)	100kHz

high-frequency, low-voltage large power electronics [26]. Fig. 6 presents a Gallium Nitride (GaN) based DC-DC sub-module experimental prototype rated at 40V, 800W, and 20A.

Circuit parameters of the DC-DC sub-module are shown in table 1.

The snubber losses of the GaN device can be reduced significantly, since its output junction capacitance is about 1/3 of the Si devices in the case of the same operating power. The bidirectional efficiency curves of the DC-DC sub-module are shown in Fig. 7.

Since the on-state resistor $R_{\mathrm{ds(on)}}$ of the device raises with operating junction temperature, the value of $R_{\mathrm{ds(on)}}$ under 90°C is 1.7 times that under 25°C junction temperature. It can be inferred that the unsatisfied design in heat dissipation leads to excessive conducting loss of GaN device. Thus, the improvement of heat dissipation design will be beneficial to the efficiency. The efficiency of PSFB DC-DC on the BOOST operation mode is lower than that of on the BUCK mode for two reasons. 1. The soft switching of 8 devices in PSFB is not achieved on the BOOST mode, increasing the switching loss. 2. The ring energy on the BOOST mode absorbed by the active clamp absorption circuit is higher than on the BUCK mode. The full load bidirectional waveform are shown in Fig. 8.

VI. THE SIMULATION OF THE SPPC-BESS

Simulation model is established to verify the dynamic behavior and the equalization of the SPPC-BESS, using Simscape Power System toolbox on MATLAB Simulink platform. The actual switch circuit in one DC-DC sub-module consists of two H-bridge circuits and a high-frequency transformer cause the numerous number of devices in the model. Then, the simulation process is too slow to debug. This article uses an equivalent DC transformer to replace the switch circuit in the DC-DC sub-modules, reducing the simulation code. The equivalent DC transformer is an average model of switch

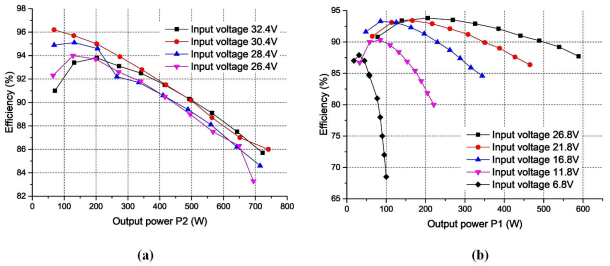

FIGURE 7. Bidirectional efficiency experiment result of 800W PSFB under different input voltage. (a) The efficiency on the BUCK mode. (b) The efficiency on the BOOST mode.

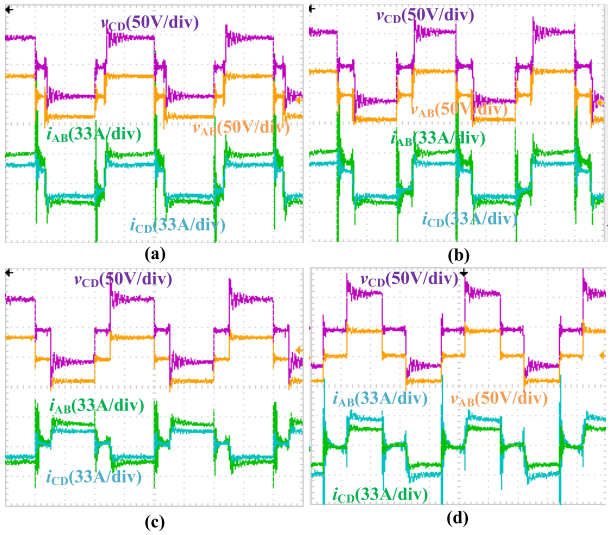

FIGURE 8. Transformer voltage and current waveform under different input voltage. The times is 5us/div. (a) Operate at 34V input and 40V output on the buck mode. (b) Operate at 38V input and 40V output on the buck mode. (c) Operate at 34V input and 40V output on the boost mode. (d) Operate at 38V input and 40V output on the boost mode.

devices [27]. The mathematical describe of the dual port of the DC transformer is in accordance with (9).

Then, the running speed of the SPPC-BESS simulation model is improved. The simulation parameters are the same as in Table 1. The grouping number is 3.

The transient response current of DC power line is shown in Fig. 9. The current waveform under step reference of the SPPC-BESS is shown in Fig. 9 (a). The settling time of i_{DC} is about 2ms when the reference signal change from 0A to 60A (or from 60A to -60A). Fig. 9 (b). shows the sine response wave. The amplitude of i_{DC} attenuates and the phase lag behind as the frequency of the reference sine signal rises. The magnitude of i_{DC} is about 43A at 800Hz, which is about 0.707 times the reference value 60A. This frequency can be defined as the cut-off frequency of the SPPC-BESS so that the bandwidth of the SPPC-BESS is 800Hz.

In the actual SPPC-BESS, one battery monitor system (BMS) is integrated with the DC-DC sub-module control system for one battery pack, judging its cut-off condition for discharging or charging. When one cell voltage reaches the upper or lower limit voltage, the battery pack stops charging and discharging by the DC-DC sub-module.

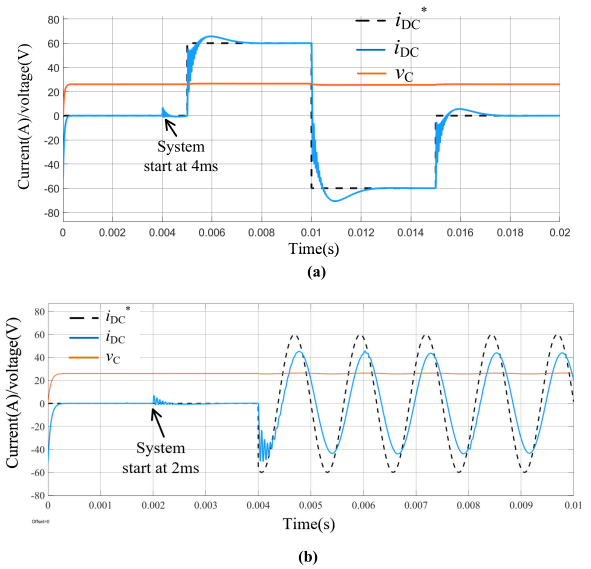

FIGURE 9. The current waveform of the SPPC-BESS. (a) The current waveform under step reference. (b) The current waveform under sine reference.

TABLE 3. Simulation parameters of the 2 situations.

Situation 1		Situation 2	
Initial SOC	0.5	$Q_{\mathrm{i}}^{\max}$	10Ah
$Q_1^{\max}$	30Ah	Initial SOC of battery pack 1	0.6
$Q_2^{\max}$	20Ah	Initial SOC of battery pack 2	0.5
$Q_3^{\max}$	10Ah	Initial SOC of battery pack 3	0.4

In simulation model the cut-off condition of battery pack is judged by the battery pack's residual discharging (or charging) capacity. When $Q_{\mathrm{i}}^{\mathrm{D}} = 0$ (or $Q_{\mathrm{i}}^{\mathrm{C}} = 0$), the battery pack i stops discharging (or charging).

The simulation parameters are listed under two situations, which are shown in Table 3. The initial SOCs of the battery packs are the same, and the maximum available capacity are different in situation 1. Whereas, the initial SOCs are different, and the maximum available capacities are the same in situation 2.

The discharging (or charging) current of the SPPC-BESS is 60A; The operation results of the SPPC-BESS with active equalization strategy are shown in Fig. 10 and Fig. 11.

The equalization strategy is executed every 1s when the currents in the battery packs are assigned. All of the battery packs are fully discharged (or charged) at the end of operation simultaneously. The distributed control method proposed in this article with active equalization can solve the available capacities and the SOC inconsistent of series-connected battery packs.

VII. ENERGY UTILIZE ANALYSIS OF THE SPPC-BESS

A. THE TOTAL POWER LOSS OF THE CONVERTER

This article supposes that the efficiency of the conventional high-voltage large-power non-isolated DC-DC converter η_{con} is 99%; the efficiency of the isolated DC-DC sub-module η_{iso} is 96%; The efficiency of the non-isolated DC-DC sub-module power converter η_{niso} is 98%;

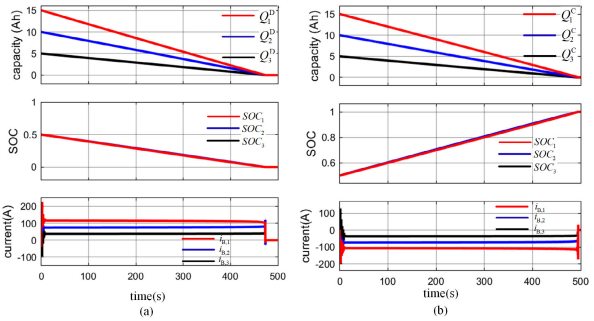

FIGURE 10. The operation result of the SPPC-BESS simulation model with active equalization strategy under situation 1. (a) The residual discharging capacity and current of 3 battery packs on discharging. (b) The residual charging capacity and current of 3 battery packs on charging.

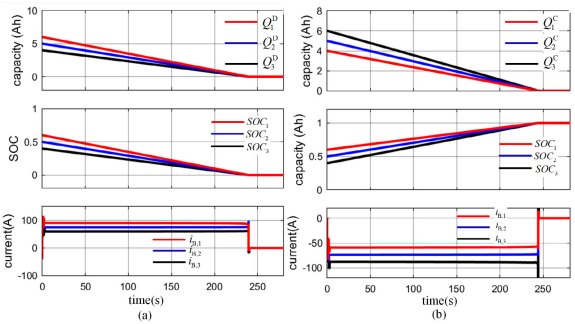

FIGURE 11. The operation result of the SPPC-BESS simulation model with active equalization strategy under situation 2. (a) The residual discharging capacity and current of 3 battery packs on discharging. (b) The residual charging capacity and current of 3 battery packs on charging.

The parameter of BESS is shown in TABLE 1. The total power losses of the four types of the power converter are compared, including the conventional converter (Case 1), the input series and output series (ISOS) isolated modular converter (Case 2), the input series and the output series (ISOS) non-isolated modular converter (Case 3), and the SPPC (Case 4). The power loss of the 4 cases are calculated in (52)-(55).

In particular, the power loss of SPPC has been calculated in section IV, where the configuration of the SPPC-BESS is "$\delta = 3.2$, n = 3".

Case 1:

$$p_{\mathrm{loss1}} = P_{\mathrm{N}} \cdot (1 - \eta_{\mathrm{con}}) = 6.6k\mathrm{W} \cdot (1 - 0.99) = 66W \quad (52)$$

where p_{loss1} is the total power loss of the conventional converter. P_{N} is the rated power of the BESS.

Case 2:

$$p_{\mathrm{loss2}} = P_{\mathrm{N}} \cdot (1 - \eta_{\mathrm{iso}}) = 6.6k\mathrm{W} \cdot (1 - 0.96) = 264W \quad (53)$$

where p_{loss2} is the total power loss of the ISOP isolated modular converter.

Case 3:

$$p_{\mathrm{loss3}} = P_{\mathrm{N}} \cdot (1 - \eta_{\mathrm{niso}}) = 6.6k\mathrm{W} \cdot (1 - 0.98) = 132W \quad (54)$$

TABLE 4. Analysis of the EUE on the 4 cases.

Cycle	0	300	600	900	1200	1500	1800
μ(Ah)	60	58	56	54	52	50	48
σ(Ah)	0	0.3	0.6	0.9	1.2	1.5	1.8
$Q_1^{\max}$(Ah)	60	59	56	54	51	49	47
$Q_2^{\max}$(Ah)	60	57	55	52	50	47	45
$Q_3^{\max}$(Ah)	60	58	56	54	52	50	48
EUE of case 1	0.98	0.9329	0.8858	0.8388	0.7917	0.7446	0.6975
EUE of case 2	0.95	0.908	0.8659	0.8239	0.7819	0.7398	0.6978
EUE of case 3	0.97	0.9271	0.8842	0.8413	0.7983	0.7554	0.7125
EUE of case 4	0.9732	0.9301	0.8871	0.844	0.8009	0.7579	0.7148

where p_{loss3} is the power loss of the non-isolated modular converter.

The full power DC-DC converter operates at the rated power, and the operating loss is equal to the product of the fixed efficiency and power. However, the SPPC-BESS operation mode is different from the conventional full power BESS. The output voltage changes in a wide scope during discharging or charging. This feather leads to a changeable efficiency and operation power. In order to evaluate the loss more accurately, we take the average of the product of efficiency and power at the beginning and endpoint of discharging as the loss of the SPPC as shown in (55).

Case 4:

$$p_{\text{loss4}} = \frac{(1-\eta_1)\cdot \text{P}_{\text{SPPC1}} + (1-\eta_2)\cdot \text{P}_{\text{SPPC2}}}{2} = 111W \tag{55}$$

where p_{loss4} is the average power loss of the SPPC during discharge. P_{SPPC1} is the operation power of the SPPC at the beginning of discharge where SOC = 100% and v_{C} reaches its minimum value. P_{SPPC2} is operation power of the SPPC at the endpoint of discharge where SOC = 0% and v_{C} reach its maximum value. η_1 is the bidirectional average efficiency simulation result at P_{SPPC1}. η_2 is the bidirectional average efficiency simulation result at P_{SPPC2}.

The SPPC achieves the lowest loss among the 3 types of modular converters since its partial power feature. However the power loss of the SPPC is slightly higher than the conventional converter.

B. THE EUE OF THE BESS

Assuming there are 36 batteries in the BESS. The aging information of Li-ion cells in different stages include cycle times, mean and standard deviation of the batteries' capacity. These aging information come from the experiment of 100 LiFePO_4 at 60Ah for 1500 cycle times [16], which can be used in this article to describe the capacity deterioration of the aging process approximatively. The capacities of batteries fits a Gaussian distribution. All of the batteries in the BESS were randomly divided into 3 groups. $Q_{\text{i}}^{\max}$ is the minimum value among all of the batteries' capacity in battery pack i. The theoretical EUEs of the 4 cases as the increase of cycle times are calculated, listed in TABLE 4.

The theoretical calculation reveals that the EUE of the 4 cases decreases with the discharging and charging cycle times. The SPPC-BESS' EUE becomes the highest among these cases after the 600th cycle times. The EUE of the SPPC-BESS is improved by 1.7% compared to the conventional converter when the average maximum available capacities attenuate to 80% of the initial capacity at 1500th cycle times. Whereas the conventional converter' EUE becomes the lowest.

The theoretical calculation results show that the EUE of the SPPC-BESS will surpass that of conventional BESS when the cycle times close to half the cycle life.

VIII. CONCLUSION

With lower cost and power loss, the SPPC-BESS is significant to replace the conventional BESS by shrink the converter design power. This article solve the basic control problem and give an optimal design scheme for high voltage and large power SPPC-BESS. A 800W PSFB bidirectional prototype is provided to verify the efficiency of the DC-DC sub-module. The simulation model of a 6.6kW SPPC-BESS is established to verify the dynamic characteristics and equalization results. Future research will focus on improving reliability and optimal equalization strategy.

REFERENCES

[1] B. Dunn, H. Kamath, and J.-M. Tarascon, "Electrical energy storage for the grid: A battery of choices," *Science*, vol. 334, no. 6058, pp. 928–935, 2011.

[2] N. Kawakami, "Development and field experiences of stabilization system using 34 MW NAS batteries for a 51 MW wind farm," in *Proc. IEEE Int. Symp. Ind. Electron.*, Jul. 2010, pp. 2371–2376.

[3] D. N. Anse, M. Dubarry, B. Liaw, M. Garcíac, and M. González, "Fast charging technique for high power LiFePO_4 batteries: A mechanistic analysis of aging," *J. Power Sources*, vol. 321, pp. 201–209, Jul. 2016.

[4] M. Yilmaz and P. T. Krein, "Review of battery charger topologies, charging power levels, and infrastructure for plug-in electric and hybrid vehicles," *IEEE Trans. Power Electron.*, vol. 28, no. 5, pp. 2151–2169, May 2013.

[5] L. Cupelli, N. Barve, and A. Monti, "Optimal sizing of data center battery energy storage system for provision of frequency containment reserve," in *Proc. 43rd Annu. Conf. Ind. Electron. Soc.*, Oct. 2017, pp. 7185–7190.

[6] Z. Li, S. Hoshina, N. Satake, and M. Nogi, "Development of DC/DC converter for battery energy storage supporting railway DC feeder systems," *IEEE Trans. Ind. Appl.*, vol. 52, no. 5, pp. 4218–4224, Sep. 2016.

[7] V. Vaquero, E. Repiso, A. Sanfeliu, and J. Vissers, "Low cost, robust and real time system for detecting and tracking moving objects to automate cargo handling in port terminals," in *Proc. 2nd Iberian Robot. Conf.*, 2016, pp. 491–502.

[8] S. Su, X. Zeng, S. Song, M. Lin, H. Dai, W. Yang, and C. Hu, "Positioning accuracy improvement of automated guided vehicles based on a novel magnetic tracking approach," *IEEE Intell. Transp. Syst. Mag.*, vol. 12, no. 4, pp. 138–148, Winter 2020.

[9] B. Zhao, R. Ran, M. Liu, and Z. Shao, "A comprehensive review of $\text{Li}_4\text{Ti}_5\text{O}_{12}$-based electrodes for lithium-ion batteries: The latest advancements and future perspectives," *Mater. Sci. Eng., R, Rep.*, vol. 98, pp. 1–71, Dec. 2015.

[10] B. Scrosati and J. Garche, "Lithium batteries: Status, prospects and future," *J. Power Sources*, vol. 195, no. 9, pp. 2419–2430, May 2010.

[11] Sungrow Power Supply. *ST101CP-50HV*. [Online]. Available: https://www.sungrowpower.com/index.php?s=/Home/Business/product_detail/id/276.html

[12] Sungrow Power Supply. *ST3727KWH(L)-D1250HV+SG-3125HV-MV*. [Online]. Available: https://www.sungrowpower.com/index.php?s=/Home/Business/product_detail/id/266.html

[13] X. Xu, J. Mi, M. Fan, K. Yang, H. Wang, J. Liu, and H. Yan, "Study on the performance evaluation and echelon utilization of retired LiFePO_4 power battery for smart grid," *J. Cleaner Prod.*, vol. 213, pp. 1080–1086, Mar. 2019.

[14] W. Li and X. He, "Review of nonisolated high-step-up DC/DC converters in photovoltaic grid-connected applications," *IEEE Trans. Ind. Electron.*, vol. 58, no. 4, pp. 1239–1250, Apr. 2011.
[15] W. Diao, N. Xue, V. Bhattacharjee, J. Jiang, O. Karabasoglu, and M. Pecht, "Active battery cell equalization based on residual available energy maximization," *Appl. Energy*, vol. 210, pp. 690–698, Jan. 2018.
[16] W. P. Diao, "Flexible grouping for enhanced energy utilization efficiency in battery energy storage systems," *Energies*, vol. 9, p. 15, Jul. 2016.
[17] P. S. Shenoy, K. A. Kim, B. B. Johnson, and P. T. Krein, "Differential power processing for increased energy production and reliability of photovoltaic systems," *IEEE Trans. Power Electron.*, vol. 28, no. 6, pp. 2968–2979, Jun. 2013.
[18] S. Qin, S. T. Cady, and A. D. Dominguez-Garcia, "A distributed approach to maximum power point tracking for photovoltaic submodule differential power processing," *IEEE Trans. Power Electron.*, vol. 30, no. 4, pp. 2024–2040, Apr. 2015.
[19] C. Liu, D. Li, Y. Zheng, and B. Lehman, "Modular differential power processing (mDPP)," in *Proc. IEEE 18th Workshop Control Modeling Power Electron. (COMPEL)*, Stanford, CA, USA, Jul. 2017, pp. 1–7.
[20] M. Shousha, T. McRae, A. Prodić, V. Marten, and J. Milios, "Design and implementation of high power density assisting step-up converter with integrated battery balancing feature," *IEEE J. Emerg. Sel. Topics Power Electron.*, vol. 5, no. 3, pp. 1068–1077, Sep. 2017.
[21] S. Inoue and H. Akagi, "A bidirectional DC–DC converter for an energy storage system with galvanic isolation," *IEEE Trans. Power Electron.*, vol. 22, no. 6, pp. 2299–2306, Nov. 2007.
[22] M. N. Kheraluwala, R. W. Gascoigne, D. M. Divan, and E. D. Baumann, "Performance characterization of a high-power dual active bridge DC-to-DC converter," *IEEE Trans. Ind. Appl.*, vol. 28, no. 6, pp. 1294–1301, Nov./Dec. 1992.
[23] W. Chen, P. Rong, and Z. Lu, "Snubberless bidirectional DC–DC converter with new CLLC resonant tank featuring minimized switching loss," *IEEE Trans. Ind. Electron.*, vol. 57, no. 9, pp. 3075–3086, Sep. 2010.
[24] H. He, R. Xiong, and J. Fan, "Evaluation of lithium-ion battery equivalent circuit models for state of charge estimation by an experimental approach," *Energies*, vol. 4, no. 4, pp. 582–598, 2011.
[25] J.-W. Kim, H.-S. Choi, and B. Hyung Cho, "A novel droop method for converter parallel operation," *IEEE Trans. Power Electron.*, vol. 17, no. 1, pp. 25–32, Jan. 2002.
[26] J. Millán, P. Godignon, X. Perpiñá, A. Pérez-Tomás, and J. Rebollo, "A survey of wide bandgap power semiconductor devices," *IEEE Trans. Power Electron.*, vol. 29, no. 5, pp. 2155–2163, May 2014.
[27] Q. M. Li, F. C. Lee, and M. M. Jovanovic, "Large-signal transient analysis of forward converter with active-clamp reset," *IEEE Trans. Power Electron.*, vol. 17, no. 1, pp. 15–24, Jan. 2002.
[28] J. Hu, Y. Zhang, S. Cui, and P. Joebges, "A partial-power regulated hybrid modular DC-DC converter to interconnect MVDC and LVDC grids," *Proc. IEEE 10th Int. Symp. Power Electron. Distrib. Gener. Syst. (PEDG)*, Jun. 20199, pp. 1030–1035.
[29] X. Fei, R. Y. Yu, and A. Huang, "Fractional converter for high efficiency high power battery energy storage system," in *Proc. IEEE Energy Convers. Congr. Expo.*, Oct. 2017, pp. 5144–5150.
[30] M. C. Mira, Z. Zhang, K. L. Jorgensen, and M. A. E. Andersen, "Fractional charging converter with high efficiency and low cost for electrochemical energy storage devices," *IEEE Trans. Ind. Appl.*, vol. 55, no. 6, pp. 7461–7470, Nov. 2019.
[31] V. M. Iyer, S. Gulur, S. Bhattacharya, and R. Ramabhadran, "A partial power converter interface for battery energy storage integration with a DC microgrid," in *Proc. IEEE Energy Convers. Congr. Expo. (ECCE)*, Sep. 2019, pp. 5783–5790.
[32] J. S. Artal-Sevil, C. Bernal-Ruiz, and J. Anzol, "Partial power processing architecture applied to a battery energy storage system," in *Proc. IEEE Vehicle Power Propuls. Conf.*, Oct. 2020, pp. 1–6.
[33] F. Gao, X. Gu, Z. Ma, and C. Zhang, "Redistributed pulsewidth modulation of MMC battery energy storage system under submodule fault condition," *IEEE Trans. Power Electron.*, vol. 35, no. 3, pp. 2284–2294, Mar. 2020.
[34] H. Liang, L. Guo, J. Song, Y. Yang, W. Zhang, and H. Qi, "State-of-Charge balancing control of a modular multilevel converter with an integrated battery energy storage," *Energies*, vol. 11, no. 4, p. 873, Apr. 2018.
[35] B. Xu, H. Tu, Y. Du, H. Yu, H. Liang, and S. Lukic, "A distributed control architecture for cascaded H-Bridge converter with integrated battery energy storage," *IEEE Trans. Ind. Appl.*, vol. 57, no. 1, pp. 845–856, Jan. 2021.

KAIYUAN ZHENG was born in Beijing, China. She received the M.S. degree in electrical engineering from the North China University of Technology, Beijing, in 2013. She is currently pursuing the Ph.D. degree with Beijing Jiaotong University. From 2013 to 2015, she was an Engineer at the Institute of Opto-Electronics, Chinese Academy of Sciences. Her research interests include battery pack application technology, motor drives, and power electronics.

WEIGE ZHANG was born in Gansu, China. He received the M.S. and Ph.D. degrees in electrical engineering from Northern Jiaotong University, Beijing, China, in 1997 and 2013, respectively. From 1993 to 1994, he was an Engineer with Hohhot Railway Bureau. He is currently a Professor with the School of Electrical Engineering, Beijing Jiaotong University. His research interests include battery pack application technology, power electronics, and intelligent distribution systems.

XUEZHI WU (Member, IEEE) received the B.S. and M.S. degrees in electrical engineering from Beijing Jiaotong University, Beijing, China, in 1996 and 1999, respectively, and the Ph.D. degree in electrical engineering from Tsinghua University, Beijing, in 2002. He is currently an Associate Professor with the Department of Electrical Engineering, Beijing Jiaotong University. His current research interests include microgrids, wind power generation systems, power converters for renewable generation systems, power quality, and motor control.

LONG JING received the B.S., M.S., and Ph.D. degrees in electrical engineering from Beijing Jiaotong University, Beijing, China, in 2000, 2002, and 2008, respectively. He is currently an Associate Professor with the Department of Electrical Engineering, Beijing Jiaotong University. His current research interests include renewable energy generation systems, microgrid, modular multilevel converters, dc grids, and power electronics for high-voltage direct current applications.